



Lattice modulation induced by magnetic order in the magnetoelectric helimagnet $\text{Ba}_{0.5}\text{Sr}_{1.5}\text{Zn}_2\text{Fe}_{12}\text{O}_{22}$

T. Asaka,^{1,2,3} X. Z. Yu,^{1,*} Y. Hiraoka,⁴ K. Kimoto,¹ T. Hirayama,² T. Kimura,⁴ and Y. Matsui¹

¹Advanced Nanocharacterization Center, National Institute for Materials Science (NIMS), Tsukuba 305-0044, Japan

²Nanostructures Research Laboratory, Japan Fine Ceramics Center (JFCC), Nagoya 456-8587, Japan

³Department of Materials Science and Engineering, Nagoya Institute of Technology, Nagoya 466-8555, Japan

⁴Division of Materials Physics, Graduate School of Engineering Science, Osaka University, Toyonaka 560-8531, Japan

(Received 6 March 2011; revised manuscript received 11 April 2011; published 26 April 2011)

By means of an electron diffraction technique, crystal-lattice modulations were investigated for a hexaferrite, $\text{Ba}_{0.5}\text{Sr}_{1.5}\text{Zn}_2\text{Fe}_{12}\text{O}_{22}$, showing a helimagnetic order below $T_N = 320$ K. We observed a lattice modulation with a wave vector $\mathbf{Q} = (0, 0, 3\delta)$ below T_N . The value of δ varies between ~ 0.23 and 0.5 as a function of temperature and corresponds well to that of the magnetic modulation vector. By applying magnetic fields, $\text{Ba}_{0.5}\text{Sr}_{1.5}\text{Zn}_2\text{Fe}_{12}\text{O}_{22}$ was found to exhibit successive changes in the lattice modulation, accompanied by the modifications of the helical magnetic order. We concluded that the observed lattice modulation is induced by the helical magnetic order via exchange magnetostriction.

DOI: [10.1103/PhysRevB.83.130401](https://doi.org/10.1103/PhysRevB.83.130401)

PACS number(s): 75.85.+t, 61.05.jm, 75.25.Dk, 75.80.+q

The magnetoelectric (ME) effect observed in some spiral magnets^{1–5} is of great interest because it is attributed to the strong coupling between ferroelectricity and magnetic order. In such ME materials, the emergence of macroscopic electric polarization is widely believed to result from charge modulations driven by the spin-current mechanism, also known as the inverse Dzyaloshinskii-Moriya (DM) interaction.^{6,7} This mechanism can interpret the electric polarization with a modulation wave vector of $\mathbf{Q} = 0$ in spiral magnets with cycloidal components. In addition to the spin-current mechanism, the conventional magnetostriction sometimes cooperates in inducing the electric polarization, though it depends on the local structure and commensurability to the lattice.^{8–10} The charge modulation with $\mathbf{Q} \neq 0$ can also arise, depending on the configuration of magnetic ordering by this mechanism. It is important to note that every charge modulation is accompanied by lattice modulations. In fact, the lattice modulations with $\mathbf{Q} \neq 0$ have been observed by means of synchrotron x-ray diffraction.^{11–15} Such lattice modulations sometimes connect to or coexist with collective atomic displacements related to the electric polarization in the ferroelectric phase. In the ME materials, the lattice modulations coupled with magnetic ordering are likely to arise from the same microscopic mechanism as the electric polarization.

The discovery of the ME effect in a Y-type hexaferrite, $\text{Ba}_{2-x}\text{Sr}_x\text{Zn}_2\text{Fe}_{12}\text{O}_{22}$,³ provided a precedent for recent studies on various ME hexaferrites functioning even in low fields and/or at room temperature.^{16–19} Kimura and co-workers³ have reported that one of magnetically induced phases in $\text{Ba}_{2-x}\text{Sr}_x\text{Zn}_2\text{Fe}_{12}\text{O}_{22}$ ($x = 1.5$) exhibits ferroelectricity at low temperature. Furthermore, it is worth noting that the magnetic order in the phase, by which the ferroelectricity is induced, persists up to 320 K. This suggests that the hexaferrites are promising materials for room-temperature giant ME effects. The fundamental crystal structure of $\text{Ba}_{2-x}\text{Sr}_x\text{Zn}_2\text{Fe}_{12}\text{O}_{22}$ belongs to the space group $R\bar{3}m$, as shown in Fig. 1(a).^{20,21} This system exhibits various magnetic structures, such as ferrimagnetic (for $x \sim 0$) and antiferromagnetic (for $x \sim 1$) structures, with a function of the Sr concentration x . Particu-

larly, in the medium range of x , a helical magnetic structure appears.^{22,23} The helical magnetic structure in this system has often been considered as an alternating stacking of the large magnetic moment (L) and the short moment (S) blocks along the c axis, having a constant turn angle ϕ [Figs. 1(a) and 1(b)]. The turn angle ϕ varies with changes in x and temperature. According to neutron-diffraction studies on this system by Momozawa *et al.*,^{23,24} for $x = 1.496$ (i.e., $x \sim 1.5$), δ_m in the magnetic modulation wave vector $\mathbf{Q}_m = (0, 0, 3\delta_m)$ varies with a function of temperature. Here, the turn angle ϕ is defined by the relationship of $\phi = 2\pi\delta_m$. Moreover, by applying magnetic fields perpendicular to the c axis, the magnetic modulation varies successively in the modulation vectors from incommensurate to $\delta_m = 1/4$ commensurate modulations and with further increasing magnetic fields through the $\delta_m = 1/2$ to the $\delta_m = 1$ modulations.^{23,25} The proposed magnetic structures corresponding to those are the following: the helix and the modified helix (for incommensurate modulations); the intermediate I (for $\delta_m = 1/4$), intermediate II (for $\delta_m = 1/2$), and intermediate III (for $\delta_m = 1/2$) phases; and the collinear ferrimagnetic (for $\delta_m = 1$) phases, respectively, as shown in Fig. 1(c). It has been found that substantial ferroelectric polarization appears in the intermediate III phase.³

In this work, we investigated lattice modulations in the ME hexaferrite $\text{Ba}_{0.5}\text{Sr}_{1.5}\text{Zn}_2\text{Fe}_{12}\text{O}_{22}$ by means of electron diffraction. Detailed measurements in wide temperature and magnetic-field regions revealed that the system has lattice modulations induced by the helical magnetic order via exchange magnetostriction.

Single crystals of $\text{Ba}_{0.5}\text{Sr}_{1.5}\text{Zn}_2\text{Fe}_{12}\text{O}_{22}$ were grown by a flux method, following Ref. 26. For measurements of electron diffraction, the crystals were cut into thin plates with the c axis on wide surfaces and thinned by mechanical grinding and Ar^+ ion sputtering. The specimens were examined using two transmission electron microscopes, a conventional electron microscope, and a Lorentz electron microscope for magnetic-field and field-free measurements, respectively. Both microscopes were operated at 300 kV. During the magnetic-field measurements, magnetic fields normal to the thin plate,

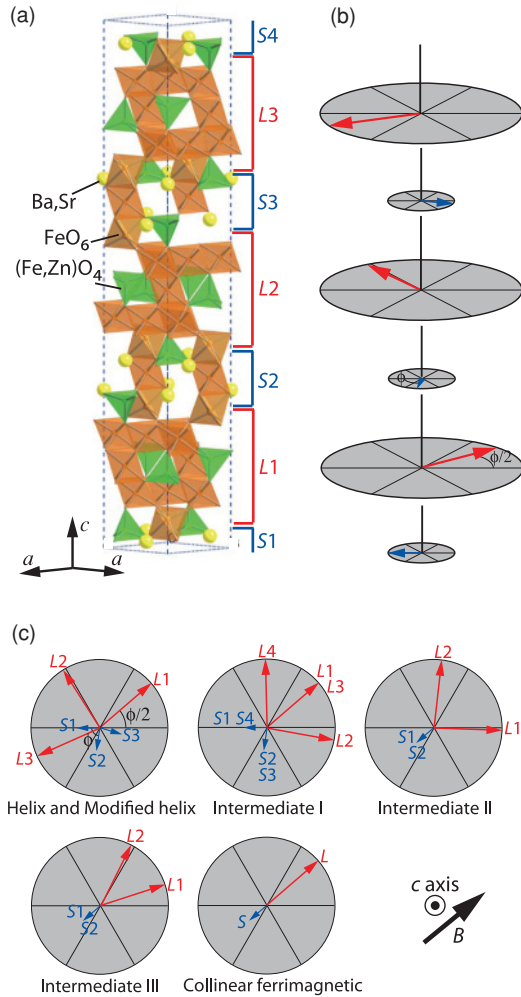


FIG. 1. (Color online) Schematic representation of (a) the crystal and (b) the magnetic structures of $\text{Ba}_{2-x}\text{Sr}_x\text{Zn}_2\text{Fe}_{12}\text{O}_{22}$. In (a), the L and S denote the large and small magnetic moments, respectively. They correspond to arrows in (b). (c) Proposed magnetic structure models for the evolution of the L and S magnetic moments by applying magnetic fields.^{23,25}

that is, perpendicular to the c axis, between 0 and 2 T were applied using pole pieces of an electromagnetic objective lens of the conventional electron microscope.²⁷ Note that in this use of the conventional electron microscope, the magnitude of the magnetic field in a low-field range might be underestimated because of the residual field of the pole pieces of the objective lens.

First, we show in Fig. 2(a) a typical electron diffraction pattern at a low temperature ($T = 19$ K) obtained without magnetic fields. We can recognize sharp weak superlattice reflections along the c^* axis, as indicated by arrows, as well as strong fundamental reflections. The superlattice reflections in the electron diffraction patterns are observable below 320 K and reveal incommensurate modulation wave vectors $\mathbf{Q}_s = (0, 0, 3\delta_s)$. The value of δ_s varies continuously between ~ 0.23 and 0.5, as a function of temperature, as shown in Figs. 2(b)–2(f). In Fig. 2(g), we plotted the temperature dependence of δ_s as well as that of δ_m reported in Ref. 24. We can recognize that the value and temperature dependence of δ_s coincide well with

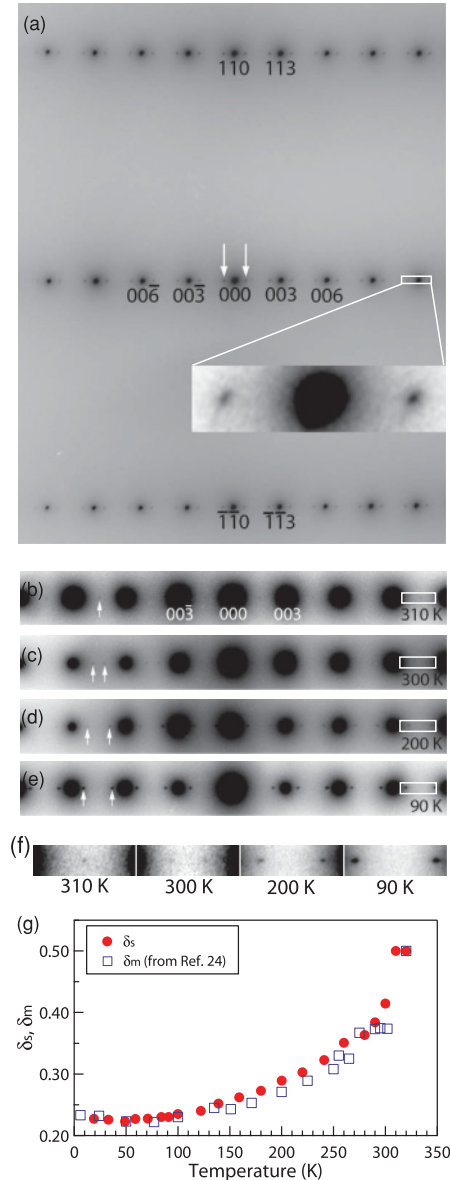


FIG. 2. (Color online) (a) $[\bar{1}10]$ -zone electron diffraction pattern of $\text{Ba}_{0.5}\text{Sr}_{1.5}\text{Zn}_2\text{Fe}_{12}\text{O}_{22}$, obtained at 19 K. Arrows indicate the superlattice reflections. Inset shows the magnified image obtained from the boxed region. The contrast of the inset image was adjusted to facilitate visualization. Temperature profiles of the $00l$ systematic electron diffraction were obtained at (b) 310 K, (c) 300 K, (d) 200 K, and (e) 90 K. (f) The magnified images obtained from the boxed regions in panels (b)–(e). The contrast of each image was independently adjusted. (g) Temperature dependence of δ_s in the lattice modulation wave vector $\mathbf{Q}_s = (0, 0, 3\delta_s)$. Temperature dependence of δ_m reported in Ref. 24 is also shown.

those of δ_m over the measured temperature range. Note that the superlattice reflections observed in the electron diffraction are generated strictly from the lattice modulation. Thus, in this compound, the crystal lattice is modulated along the c axis with the same periods as helical magnetic orders. The lattice modulations are related to the magnetic modulations with $\mathbf{Q}_s = \mathbf{Q}_m$ in this system.

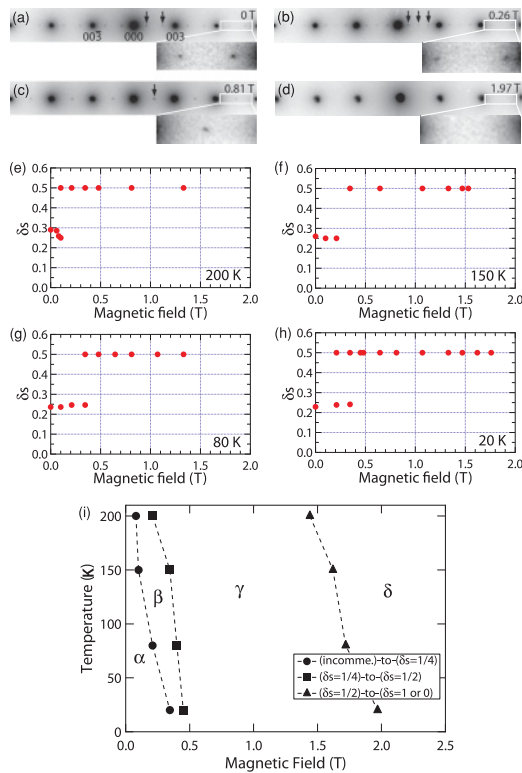


FIG. 3. (Color online) The $00l$ systematic electron-diffraction patterns obtained in the magnetic fields of (a) 0 T, (b) 0.26 T, (c) 0.81 T, and (d) 1.97 T. These were obtained at 200 K. Arrows indicate the superlattice reflections. Lower right panels of the respective figures show magnified images around the superlattice reflections. Magnetic-field dependences of δ_s are shown at temperatures of (e) 200 K, (f) 150 K, (g) 80 K, and (h) 20 K. (i) Phase diagram of $\text{Ba}_{0.5}\text{Sr}_{1.5}\text{Zn}_2\text{Fe}_{12}\text{O}_{22}$, regarding the lattice modulation and temperature. Regions α , β , γ , and δ correspond to the incommensurate, $\delta_s = 0.25$, $\delta_s = 0.5$, and $\delta_s = 0$ or 1 phases, respectively.

The lattice modulation was found to be variable by applying magnetic fields. As a typical example of the modulation behavior, in Figs. 3(a)–3(d), we show the $00l$ -systematic electron diffraction patterns at 200 K, obtained in various magnetic fields. At this temperature, the modulation wave vector is incommensurate with $\delta_s \sim 0.29$ in zero fields. When a magnetic field is applied, the δ_s value approaches 0.25, which indicates the commensurate lattice modulation. Concomitantly with reaching $\delta_s = 0.25$, the superlattice reflections with $\delta_s = 0.5$ appear [Fig. 3(b)]. Here, we cannot decide whether the $\delta_s = 0.5$ superlattice reflections are of unique \mathbf{Q}_s or the second orders of the $\delta_s = 0.25$ superlattice reflections. By further increasing the magnetic field, the $\delta_s = 0.25$ superlattice reflections vanish, while the $\delta_s = 0.5$ superlattice reflections remain [Fig. 3(c)]. Eventually, the $\delta_s = 0.5$ superlattice reflections also vanish by applying a magnetic field of ~ 1.4 T [Fig. 3(d)]. In Figs. 3(e)–3(h), we plotted the δ_s values as functions of magnetic fields at various temperatures. Thus, we found that the application of magnetic fields causes successive phase transitions (the incommensurate \rightarrow the $\delta_s = 0.25$ commensurate \rightarrow the $\delta_s = 0.5$ commensurate \rightarrow the $\delta_s = 0$ or 1 phases). This behavior is

quite similar to that of the magnetic modulations in magnetic fields as described above [Fig. 1(c)].

Figure 3(i) shows the phase diagram representing the lattice modulations in magnetic fields. In Fig. 3(i), we plotted the phase boundaries, which were determined from the field dependences of the δ_s values. Here, the phase boundaries in the low-field range (< 0.5 T) may be inaccurate, as mentioned above. Taking this into account, we consider the phase diagram of the lattice modulation to be similar to the phase diagrams of the magnetic phases, as reported in Refs. 3 and 23. Note that one cannot distinguish between the intermediate II and III magnetic phases from the lattice modulation, because the both phases commonly exhibit the $\delta_s = 0.5$ lattice modulations.

Finally, we discuss the origin of the observed lattice modulations. The lattice modulations with $\mathbf{Q}_s = \mathbf{Q}_m$ can be presumed to resemble the lattice modulations of holmium²⁸ and dysprosium²⁹ in magnetic fields. These rare-earth metals are known to exhibit fan³⁰ or helifan³¹ spin structures in certain magnetic fields, while the proper screw (helix) spin structures appear in zero fields. The lattice modulations induced by the fan and helifan spin structures are interpreted with the conventional exchange magnetostriction.^{28,29} In these cases, the local magnetostrictions related to the local spin arrangements, where the scalar product $S_i \cdot S_j$ is spatially modified periodically with the same modulation vector as \mathbf{Q}_m , occur on the crystal lattice.⁹ This mechanism can account for the modified helix and intermediate (fan) phases in the present Y-type hexaferrite in magnetic fields. This assumption is supported by an intensity variation of the superlattice reflections for the cooling procedures in regard to magnetic fields. Figure 4(a) shows intensity profiles of the superlattice reflections $009 \pm \delta_s$ in 0.01 T at 80 K. The profiles represented with the solid and dashed lines are for the reflections obtained through zero-field cooling and field (0.01 T) cooling processes, respectively. When the sample was cooled in the magnetic field, intensities of the superlattice reflections were obviously

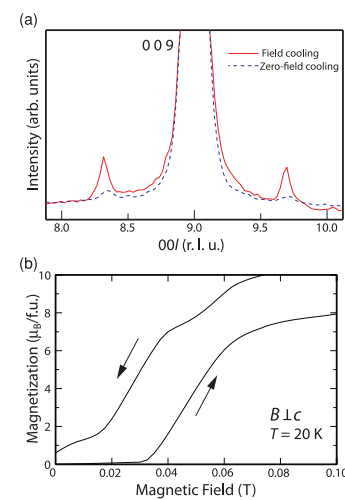


FIG. 4. (Color online) (a) Intensity profiles of the electron diffraction around the 009 reflection along $00l$ in 0.01 T at 80 K. Solid and dashed lines are profiles for field (0.01 T) cooling and zero-field cooling procedures, respectively. (b) Magnetic-field dependence of magnetization of $\text{Ba}_{0.5}\text{Sr}_{1.5}\text{Zn}_2\text{Fe}_{12}\text{O}_{22}$. The magnetic fields perpendicular to the c axis were applied at 20 K.

stronger than that in the case of the zero-field cooling process, though the δ_s values are almost the same. This suggests that coherent order of the magnetic moments, which is exhibited in the field cooling process, enhances the lattice modulation. This enhancement of the superlattice reflections can support the above assumption. However, this model is inapplicable to the proper helix magnetic structure in zero fields, because the turn angle ϕ is constant; that is, there is no spatial modification of the scalar product along the helical axis. Regarding this contradiction, we speculate that a ferromagnetic component exists in the helix phase, even when the sample is in zero fields. In fact, we observed finite remanent magnetization in the magnetization curve at low temperature, as shown in Fig. 4(b). We consider the magnetic ground state of the present Y-type hexaferrite to be a distorted helical magnetic structure with the ferromagnetic component within the ab plane rather than the proper helical one.

In conclusion, we observed lattice modulations connected with magnetic modulations of helimagnetic ordered structures in magnetoelectric $\text{Ba}_{0.5}\text{Sr}_{1.5}\text{Zn}_2\text{Fe}_{12}\text{O}_{22}$. The modulation of crystal structure varied with the same wave vectors as

that of the magnetic one as a change in temperature and with application of magnetic fields. We concluded that the lattice modulations were induced by the magnetic orders via exchange magnetostriction. Incidentally, the lattice modulation in the ferroelectric phase (intermediate III phase) was unveiled. The assumed exchange magnetostriction would not connect directly to the electric polarization. However, it might prepare the path to the ferroelectric phase. We expect to study the structural analysis, including the lattice modulation in the ferroelectric phase, in the future. Furthermore, our results that the superlattice reflections are observable in the electron diffraction provide the possibility for real-space observations of the lattice modulation in the helical magnet by electron microscopy.

We thank Y. Zhu and V. V. Volkov for their valuable discussions and J. Q. He and W. Z. Zhang for their assistance. Work by T.A. was supported by a grant from Institute of Ceramics Research and Education, Nagoya Institute of Technology. Work by Y.H. and T.K. was supported by KAKENHI (Grants No. 20674005 and No. 20001004), MEXT, Japan.

*Present address: Correlated Electron Research Group, RIKEN-ASI, Wako 351-0198, Japan.

¹T. Kimura, T. Goto, H. Shintani, K. Ishizaka, T. Arima, and Y. Tokura, *Nature (London)* **426**, 55 (2003).

²N. Hur, S. Park, P. A. Sharma, J. S. Ahn, S. Guha, and S.-W. Cheong, *Nature (London)* **429**, 392 (2004).

³T. Kimura, G. Lawes, and A. P. Ramirez, *Phys. Rev. Lett.* **94**, 137201 (2005).

⁴Y. Yamasaki, S. Miyasaka, Y. Kaneko, J.-P. He, T. Arima, and Y. Tokura, *Phys. Rev. Lett.* **96**, 207204 (2006).

⁵T. Kimura, J. C. Lashley, and A. P. Ramirez, *Phys. Rev. B* **73**, 220401(R) (2006).

⁶H. Katsura, N. Nagaosa, and A. V. Balatsky, *Phys. Rev. Lett.* **95**, 057205 (2005).

⁷I. A. Sergienko and E. Dagotto, *Phys. Rev. B* **73**, 094434 (2006).

⁸I. A. Sergienko, C. Şen, and E. Dagotto, *Phys. Rev. Lett.* **97**, 227204 (2006).

⁹C. Jia, S. Onoda, N. Nagaosa, and J. H. Han, *Phys. Rev. B* **76**, 144424 (2007).

¹⁰M. Mochizuki, N. Furukawa, and N. Nagaosa, *Phys. Rev. Lett.* **105**, 037205 (2010).

¹¹T. Arima, Y. Yamasaki, T. Goto, S. Iguchi, K. Ohgushi, S. Miyasaka, and Y. Tokura, *J. Phys. Soc. Jpn.* **76**, 023602 (2007).

¹²T. Kimura, S. Ishihara, H. Shintani, T. Arima, K. T. Takahashi, K. Ishizaka, and Y. Tokura, *Phys. Rev. B* **68**, 060403(R) (2003).

¹³D. Higashiyama, S. Miyasaka, N. Kida, T. Arima, and Y. Tokura, *Phys. Rev. B* **70**, 174405 (2004).

¹⁴T. Arima, T. Goto, Y. Yamasaki, S. Miyasaka, K. Ishii, M. Tsubota, T. Inami, Y. Murakami, and Y. Tokura, *Phys. Rev. B* **72**, 100102(R) (2005).

¹⁵Y. Yamasaki, H. Sagayama, N. Abe, T. Arima, K. Sasai, M. Matsuura, K. Hirota, D. Okuyama, Y. Noda, and Y. Tokura, *Phys. Rev. Lett.* **101**, 097204 (2008).

¹⁶S. Ishiwata, Y. Taguchi, H. Murakawa, Y. Onose, and Y. Tokura, *Science* **319**, 1643 (2008).

¹⁷Y. Kitagawa, Y. Hiraoka, T. Honda, T. Ishikura, H. Nakayama, and T. Kimura, *Nat. Mater.* **9**, 797 (2010).

¹⁸S. H. Chun, Y. S. Chai, Y. S. Oh, D. Jaiswal-Nagar, S. Y. Haam, I. Kim, B. Lee, D. H. Nam, K.-T. Ko, J.-H. Park, J.-H. Chung, and K. H. Kim, *Phys. Rev. Lett.* **104**, 037204 (2010).

¹⁹Y. Tokunaga, Y. Kaneko, D. Okuyama, S. Ishiwata, T. Arima, S. Wakimoto, K. Kakurai, Y. Taguchi, and Y. Tokura, *Phys. Rev. Lett.* **105**, 257201 (2010).

²⁰J. Smit and H. P. J. Wijn, *Ferrites* (Phillips Technical Library, Eindhoven, 1959).

²¹P. B. Braun, Philips Res. Rep. **12**, 491 (1957).

²²U. Enz, *J. Appl. Phys.* **32**, 22S (1961).

²³N. Momozawa and Y. Yamaguchi, *J. Phys. Soc. Jpn.* **62**, 1292 (1993).

²⁴N. Momozawa, Y. Yamaguchi, H. Takei, and M. Mita, *J. Phys. Soc. Jpn.* **54**, 771 (1985).

²⁵N. Momozawa, Y. Yamaguchi, H. Takei, and M. Mita, *J. Phys. Soc. Jpn.* **54**, 3895 (1985).

²⁶N. Momozawa, M. Mita, and H. Takei, *J. Cryst. Growth* **83**, 403 (1987).

²⁷V. V. Volkov, D. C. Crew, Y. Zhu, and L. H. Lewis, *Rev. Sci. Instrum.* **73**, 2298 (2002).

²⁸H. Ohsumi and K. Tajima, *J. Phys. Soc. Jpn.* **67**, 1883 (1998).

²⁹Y. Kida, K. Tajima, Y. Shinoda, K. Hayashi, and H. Ohsumi, *J. Phys. Soc. Jpn.* **68**, 650 (1999).

³⁰T. Nagamiya, K. Nagata, and Y. Kitano, *Prog. Theor. Phys.* **27**, 1253 (1962).

³¹J. Jensen and A. R. Mackintosh, *Phys. Rev. Lett.* **64**, 2699 (1990).